OPEN

Microsystems & Nanoengineering (2018) **4**, 17087; doi:10.1038/micronano.2017.87

www.nature.com/micronano

ARTICLE

Combined flow-focus and self-assembly routes for the formation of lipid stabilized oil-shelled microbubbles

Adam H. Churchman[1], Victoria Mico[1], Julia Gala de Pablo[1], Sally A. Peyman[1], Steven Freear[2] and Stephen D. Evans[1]

Lipid and polymer stabilized microbubbles are used in medicine as contrast agents for ultrasound imaging and are being developed for the delivery of water soluble drugs to diseased areas of the body. However, many new therapeutics exhibit poor water solubility or stability, which has led to the requirement for the development of effective hydrophobic drug delivery systems. This study presents a new method to produce microbubbles coated with an oil layer capable of encapsulating hydrophobic drugs and suitable for targeted, triggered drug release. This new method utilizes highly controllable flow-focusing microfluidics with lipid oil nanodroplets self-assembling and spreading at gas–aqueous interfaces. Oil layer inside microbubbles were produced with diameters of 2.4 ± 0.3 μm (s.d., 1.6 μm) and at concentrations up to 10^6 bubbles per milliliter. The mechanism of oil layer inside microbubble assembly and stability were characterized using methods including contact angle measurements, quartz crystal microbalance with dissipation monitoring and fluorescence resonance energy transfer imaging.

Keywords: microbubbles; microfluidics; drug-delivery; hydrophobic; lipid-coated; oil-shelled

Microsystems & Nanoengineering (2018) **4,** 17087; doi:10.1038/micronano.2017.87; Published online: 26 February 2018

INTRODUCTION

It has been estimated that up to 40% of all newly developed drugs have poor water solubility.[1,2] Many drugs also show poor stability in water. Thus, while many of these drugs have shown good results *in vitro* their efficacy is reduced *in vivo* and in some cases have been show to increase toxicity toward healthy tissue[2]. For example, drugs such as Combretastatin A4, a vascular disrupting agent proposed for the treatment of colorectal cancer, have proven difficult to deliver effectively due to their hydrophobicity[3], while drugs such as the anti-cancer agent Decitabine, a DNA methyltransferase inhibitor, have been shown to undergo rapid decomposition in water to inactive products[4]. A number of hydrophobic drug encapsulation systems have been investigated previously, such as porous nanoparticles[1,5], sub-micron oil emulsions[6], and micelles[7]. The release mechanisms of these systems can be either passive, for example, due to drug leakage from the carrier, or active, due to environmental-triggered release, for example, in response to local temperature or pH[8,9]. However, such mechanisms often lead to unpredictable drug release profiles when applied *in vivo*[10]. Therefore, a hydrophobic drug delivery system with a controlled, externally activated, triggered release mechanism could offer a considerable advantage over existing technologies.

Lipid and polymer-shelled microbubbles (MBs) have been used as contrast enhancing agents in ultrasound (US) imaging for over 30 years[11]. The compressibility of their gas core combined with its high acoustic impedance mismatch against surrounding blood plasma leads to a large scattering cross-section so that MBs provide a higher echogenicity than tissue interfaces[12–14]. This makes MBs a powerful tool in diagnostic US imaging of the cardiovascular system and organs. MBs have more recently been shown to enhance therapeutic delivery[15], making them promising 'theranostic' agents, with both 'diagnostic' and 'therapeutic' capabilities. US destruction pulses can be used to trigger the release of encapsulated/attached drug payload by destroying the MB vehicle at the target. Alternatively, stable cavitation of MBs may be used to drive sonoporation of the nearby cells and stream fluid around the MBs, thereby aiding drug uptake, and MB destruction can lead to 'microjets,' which are able to pierce endothelial lining allowing improved efficacy of drug injection[15,16].

To date, these dual functional MBs have been formed in a number of designs. MBs have been loaded with DNA/RNA in the lipid shell[17–19]. They have been decorated with nanobeads[18] and vesicles[14] for coating with and the encapsulation of hydrophilic species, respectively. Examples of loading have included quantum dots, luciferin, and propidium iodide[20,21]. With a simple lipid or polymer shell structure, MBs have also been co-delivered with hydrophilic species and drugs, for example, to overcome delivery across the blood–brain barrier[22] and enhance transdermal transport of insulin and heparin[23].

MBs are conventionally produced by sonication, mechanical agitation, or microfluidics, typically through the use of a gas with low water solubility and an aqueous solution of lipids or polymers. MBs are required to be smaller than 8 μm to avoid the risk of blood flow complications such as arterial embolisms[24,25]. For the production of more complex MB architectures, such as those with drug payloads and molecular targeting, microfluidic approaches offer greater control over MB size, reduced wastage of drug cargo and targeting agents, and ease of cleaning the final product[14,26]. Microfluidic-based MB preparation typically utilizes flow-focusing (FF) geometries, where a gas phase is pinched off at a nozzle to form a MB, by a continuous aqueous phase containing a surfactant

[1]School of Physics and Astronomy, University of Leeds, Woodhouse Lane, Leeds LS2 9JT, UK and [2]School of Electronic and Electrical Engineering, University of Leeds, Woodhouse Lane, Leeds LS2 9JT, UK.
Correspondence: Stephen Evans (S.D.Evans@leeds.ac.uk)
Received: 1 June 2017; revised: 14 September 2017; accepted: 28 September 2017

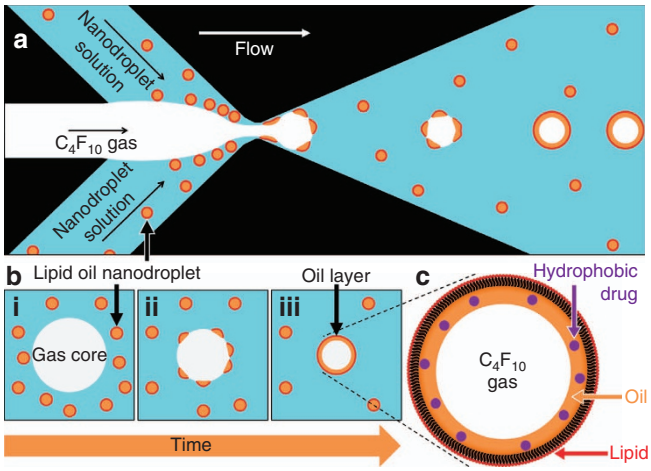

Figure 1 Schematic of the (**a**) microfluidic OLI-MB production method, (**b**(i)–(iii)) proposed mechanism of LOND adsorption and spreading at a bubble surface over time, and (**c**) final OLI-MB structure. LOND, lipid oil nanodroplets; OLI-MB, oil layer inside MB.

agent, usually lipids. Hettiarchi and Talu have previously shown high levels of size control, producing lipid-coated, perfluorocarbon core 1–5 μm MBs with polydispersity indices as low as 2–5%[27–29]. We have also developed an on-chip 'microspray regime' for MB formation, which can produce high concentrations of MBs ($>10^9$ MB mL^{-1}) with an average size of 1.5 μm[14,30].

One possible route for the incorporation of drugs onto the MB architecture is to thicken the MB shell with an oil layer, giving an oil layer inside MB (OLI-MB). These MBs would allow hydrophobic drugs to be held within the oil component, while retaining their US properties for imaging and active release. Unger *et al.*[31] were the first to incorporate an oil layer into MBs, which they termed acoustically active lipospheres (AALs). Since then AALs have been reproduced and further characterized by other groups. AALs have been produced through the mechanical agitation of lipid solution, oil (primarily soybean or triacetin), and a gas such a perfluorobutane (C_4F_{10}), resulting in MBs of 2.9 μm average diameter with a thick oil shell capable of high drug loading per MB[31], but large MB–MB variability with sizes ranging from 1 to 10 μm and drug loading being inconsistent between vehicles[32,33]. Oil layers can range from 500 to 1000 nm and 300 to 700 nm for triacetin and soybean oil, respectively, with some vehicles containing no gas at all[33,34]. It is thought that this large MB to MB variability is due to the production method's chaotic nature, and lack of control over gas encapsulation. In terms of their US capabilities, AALs' thick oil layer is thought to lead to viscous dampening[34]. Compared to non-oil-MBs, AALs fragmentation by US is significantly more difficult, with a high mechanical index of 0.67–2.0, and a fivefold higher pulse length being required for MB destruction[32,34]. During tests of AALs on cells, 30% of the cells were found to die from the US alone[35]. In 2009, Lentacker *et al.*[35] concluded that it remained difficult to efficiently release drugs from AALs using medically relevant US. Colombo and Edirisinghe demonstrated the production of ~50 μm multi-layered OLI-MBs through the use of coaxially arranged needles, providing more monodisperse MBs[36,37]. However, this method is in part limited by the needles' inner and outer diameters, often leading to MBs that are larger than that required for medical applications. Lee and Zhang have previously demonstrated methods for OLI-MB and multi-layered MB production using a three-phase FF system and a system of two subsequent two-phase FF nozzles, respectively[10,25,38]. However, control of three different phases on-chip is inherently difficult and often leads to poor MB yields. As depicted in Figure 1, we propose a new, simple method for the production of MBs with an internalized thin oil layer between the gas core and lipid shell, OLI-MBs. Here we produce OLI-MBs using a FF system but include an emulsion of oil nanodroplets stabilized by a lipid monolayer shell, termed lipid oil nanodroplets (LONDs), into the aqueous phase. The LONDs undergo adsorption, rupture, and spreading at the gas–water interface, leading to the formation of a tens of nanometers thick oil layer around the MB. By including the LONDs in the aqueous phase, the microfluidics is brought back to a two-phase system, permitting easier control over MB production and potentially allowing a broader range of hydrophobic solvents to be used for delivery. A combination of contact angle measurements and quartz crystal microbalance with dissipation (QCM-D) monitoring was used to identify the mechanisms of OLI-MB formation while fluorescence microscopy, including fluorescence resonance energy transfer (FRET), was used to confirm the final OLI-MB structure.

MATERIALS AND METHODS

Materials

The lipid used in this work was 1-palmitoyl-2-oleoyl-sn-glycero-3-phosphocholine (POPC), purchased from Avanti Polar Lipids (Alabaster, Al, USA). Squalane oil (Sigma-Aldrich, Dorset, UK) was used as the hydrophobic carrier phase. Phosphate-buffered saline (PBS) was prepared by dissolving one 5 g tablet of PBS powder (Life Technologies, Carlsbad, CA, USA) in 500 mL of MilliQ water and filtered through a 200 nm cellulose membrane syringe filter (Sartorius Stedim, Epsom, UK) prior to use.

Contact angles measurement and surface energy

Contact angle measurements of oil droplets at the water/lipid–air interface were performed. These were used to calculate the interfacial free energies of an OLI-MB, and to estimate the total interfacial energy of a specific OLI-MB structure compared to other conformations of oil and air in water in the presence of lipids.

A circular Teflon dish (6 cm diameter) was filled with MilliQ to allow a meniscus to form above the top of the dish walls. This meniscus was aspirated off before the dish was refilled. This was repeated a minimum of five times to remove any surface contaminants. This set up was analogous to a Langmuir Blodgett (LB) trough. POPC lipid, solubilized in chloroform at 1 mg mL^{-1}, was added gradually to the water surface. This gave surface concentrations of either no lipid or enough lipid that the surface pressure was increased to just before the lipid layer collapsed at the dish edge, which was assumed to be at the collapse pressure. The sessile drop technique was used for contact angle measurement, using a First Ten Angstroms instrument, by depositing a droplet of oil at the air–water/lipid interface using a square cut needle. Images of the oil droplet were analyzed in ImageJ to measure both the left and right contact angles. At least five droplets were measured for each lipid monolayer condition. These contact angles were used to calculate the water/lipid–oil surface tension and total surface energies, described below.

LOND production

LONDs were formed via two methods, either by tip sonication or a two-stage ultra-fine homogenization process (in a similar method to that presented by Mico *et al.*[39]). 3,3′-Dioctadecyloxacarbocyanine perchlorate (DiO), and dioctadecyl-3,3,3′,3′-tetramethylindocarbocyanine perchlorate (DiI) (Sigma-Aldrich, Dorset, UK) were encapsulated into the oil as drug mimics, and for optical quantitative purposes, by sonication for 30 min at room temperature, at a concentration of 1 mg mL^{-1}.

LOND formation via tip sonication. An aliquot of 10 mg POPC lipid was dissolved in 1:1 chloroform–methanol, dried under nitrogen in a glass vial for 30 min, and then re-dispersed in 930 μL

doi:10.1038/micronano.2017.87

of PBS (Thermo Fisher Scientific, Waltham, MA, USA). An aliquot of 70 µL of oil was added. To form a LOND emulsion, the solution was vortexed for 30 s, then tip sonicated at 200 W, 20% power, 100% duty cycle, for 15 min in a 4 °C cooled jacketed glass vessel. The LOND solution was dialysed utilizing a 100 kDa pore-size membrane for over 12 h to remove non-encapsulated fluorophore, and to reduce any excess lipid in solution until in equilibrium with the LONDs.

LOND formation via homogenization. An aliquot of 100 mg of dried lipid was re-dispersed in 3.3 mL of PBS and 700 µL of oil was added. To form an oil droplet emulsion, the solution was vortexed, coarsely homogenized with a Polytron PT1300 D (Kinematica AG, Luzern, Switzerland) at 12.5 krpm, 40 °C, and atmospheric pressure for 10 min. The emulsion was made up to 10 mL with PBS buffer and, to form a LOND emulsion, finely homogenized under high pressure in an Avestin EmulsiFlex-C5 (Avestin Europe GmbH, Mannheim, Germany) at ~175 MPa, 4 °C for 20 min. The emulsion was then filtered using a KrosFlow Research Ili Tangential Flow Filtration System (SpectrumLabs Europe, Breda, the Netherlands) at 100 kDa, 45 mL min^{-1} for at least 2 h for the same reason as dialysis above.

LOND sizing and concentration measurements were performed using a Zetasizer and NanoSight (Malvern Instruments, Malvern, UK). LONDs were typically produced at ~170 nm diameter and 10^{13} LONDs per milliliter.

QCM-D: LOND spreading mechanics

QCM-D was used to study LOND interactions with hydrophobic solid surfaces in an aqueous environment as a mimic to the air–water MB interface.

Octadecanethiol (Sigma-Aldrich, Dorset, UK) was used for coating gold-coated QCM-D crystals (Q-Sense AB, Stockholm, Sweden). Prior to the experiments, the crystals were thoroughly cleaned by UV-ozone cleaning for 20 min, followed by immersion in Decon 90 and then MilliQ while in a sonication bath, and finally vigorous agitation in isopropanol. The crystals were kept in each solution for about 10 min. This process was followed by an N_2 dry and again by UV-ozone for 20 min. Hydrophobic self-assembled monolayers were formed on the gold-coated crystals by immersion of the crystals in octadecanethiol in ethanol (1 mg mL^{-1}) for 12 h, after which they were rinsed with ethanol, to remove excess octadecanethiol, and MilliQ. For all QCM-D experiments, water contact angle measurements were performed on a control QCM-D crystal to confirm hydrophobicity, using a First Ten Angstroms instrument with MilliQ droplets.

A Q-Sense E4 (Q-Sense AB, Stockholm, Sweden) was used to monitor the interaction between the LONDs and the QCM-D crystal. Crystals were allowed to equilibrate for at least 1 h in degassed PBS, flowing at 14 µL min^{-1}. The 5th, 7th, 9th, and 11th overtones were recorded and used in the analysis. The LONDs were introduced in to the flow chambers at a dilution of 10^{12} LONDs per mL in PBS, at 140 µL min^{-1}. The flow was then stopped for ~2 h until no further frequency or dissipation changes were observed. PBS was used to rinse the system, in order to remove any unattached material (140 µL min^{-1}). The Sauerbrey and the Voigt-viscoelastic models were fitted to the above harmonics to calculate the mass adhered to the crystal during the experiment and estimate the thickness of the oil–lipid layer formed.

Microfluidic OLI-MB production

Microfluidic FF devices were designed in Leeds and fabricated by Epigem Ltd (Redcar, UK) in PMMA and SU-8, as described previously and shown schematically in Figure 1a[9]. LOND solution was diluted to 10^{12} LONDs per mL in 10% v/v glycerol, 4 mg mL^{-1} NaCl. LOND solution flow rates of 15–50 µL min^{-1} were delivered via a syringe pump (Aladdin, World Precision Instruments, Sarasota, FL, USA), passing first through a 200 nm filter (Sartorius Stedim, UK) to remove any oil that was not successfully homogenized or from LONDs that had destabilized over time. Flow of the LOND solution in the absence of MB production did not result in the formation of larger agglomerates but rather yielded oil emulsion comparable to the initial LOND solution, indicating their relative stability due to the lipid shell. Indeed, we have found these solutions to be stable for over 6 weeks[39]. C_4F_{10} gas (F2 Chemicals, Preston, UK) pressures of 20–34.5 kPa were regulated by a digital gas flow controller (Alicat Scientific, Tucson, AZ, USA). At the nozzle, the gas was pinched off and stabilized as a MB by the LOND solution. The MB solution contained 10 µL of liquid perfluorohexane (C_6F_{14}) per 1 mL of precursor MB solution to extend MB lifetime by intercalation of the C_6F_{14} into the MB shell[40]. High frame rate imaging (FASTCAM SA-X, Photron, San Diego, CA, USA) between 10 and 50 kfps, performed on an inverted light microscope (Eclipse Ti-U, Nikon, Tokyo, Japan), was used to observe single MB pinch-off and flow immediately after the nozzle during production. For size and concentration measurements, 50 µL of the MB solution, taken from the middle of the solution immediately after gentle agitation to prevent pre-concentration due to bubble buoyancy, was placed in a 120 µm deep, BSA Dorset, Sigma-Aldrich, UK) coated, glass chamber and observed under dark field (Eclipse Ti-U, Nikon, Tokyo, Japan) with an oil immersion ×100 objective.

For the determination of MB lifetime, three 50 µm deep, BSA-coated, wax sealed, glass observation chambers were prepared and the MBs were observed using dark-field microscopy, as a function of time. The MB diameter and concentration were measured using ImageJ.

OLI-MB washing

Microfluidic cell-traps were used to trap and wash larger OLI-MBs to confirm the structure of the MBs[41]. The traps were made from PDMS, and were designed to catch >5 µm MBs, to allow higher resolution imaging of OLI-MB structures. Prior to any use, the microfluidic devices were washed with 70% ethanol to remove any air, followed by 1 mL MilliQ and 1 mL of 1 mg mL^{-1} BSA in PBS at 100 µL min^{-1} to reduce non-specific binding of excess LONDs to the cell-trap walls. The MB sample was then introduced to the device at 5 µL min^{-1} over 20–30 min (allowing enough MBs to be trapped), before being washed by PBS at 10 µL min^{-1} for 30 min. All observations were made using a Confocal Laser Scanning Platform Leica TCS SP8 on a DMi8 microscope (Leica Microsystems, Milton Keynes, UK) with a 488 nm excitation laser and a 561–582 nm emission window. LAS X software was used for image capture and processing.

FRET LOND interactions on MBs

FRET was used to infer LOND destablization and LOND to LOND mixing at the MB gas–aqueous interface. Separate preparations of LONDs were made containing either a FRET donor (DiO) or a FRET acceptor (DiI) dye[42,43]. These solutions were mixed 1:1 and then diluted to 10^{12} LONDs per ml in PBS. This mixed LOND solution was then used to produce MBs microfluidically, as above. MB samples were loaded into 50 µm deep, BSA-coated glass-viewing chambers. Fluorescence was then observed on the above confocal system with a ×40 objective, using a 488 nm excitation laser, and 500–520 nm and 561–582 nm emission windows for the donor and acceptor, respectively. In order to identify the enhanced FRET fluorescence, FRET donor LOND + FRET acceptor LOND samples were compared to control donor + non-fluorescent/empty and empty + acceptor samples. As in Equation (1), the intensity at the MB surface in both control images was removed

from the donor + acceptor image to reveal the FRET signal[44,45].

$$FRET_f = FRET_i - \left(Imax_{Donor+Empty} + Imax_{Empty+Acceptor}\right) \quad (1)$$

where $FRET_f$ is the final FRET image, $FRET_i$ is the initial FRET (donor +acceptor) image, and I is the intensity.

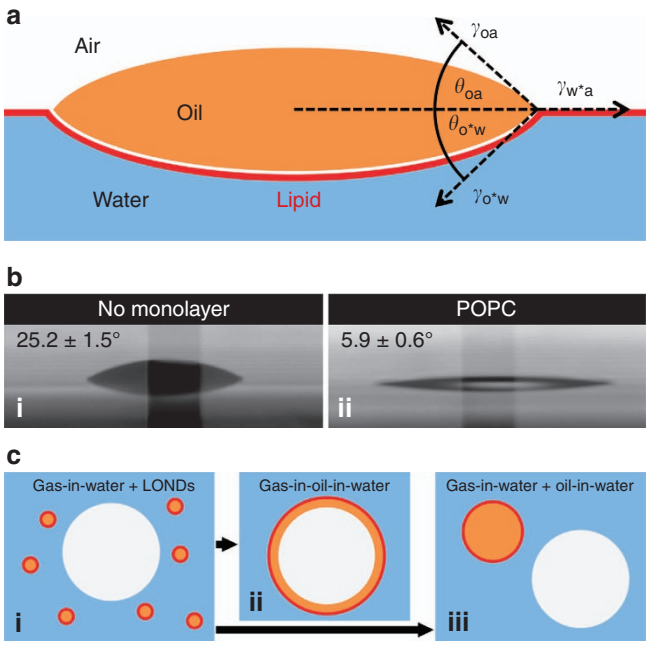

Figure 2 (**a**) A schematic of the oil/lipid/water interface, and images of (**b**) (i) a squalane oil droplet at an air/MilliQ interface and (ii) in the presence of POPC lipid, for the contact angle and total surface energy values calculated. A minimum of five droplets were imaged and their contact angles averaged, calculating standard error, for each monolayer type. (**c**) Schematic of the possible oil, gas and lipid configurations, showing (i) the initial state of LONDs around a MB without a surfactant/lipid shell, leading to (ii) an OLI-MB or (iii) the LONDs coalescing and the MB remaining unchanged. LOND, lipid oil nanodroplets; POPC, 1-palmitoyl-2-oleoyl-sn-glycero-3-phosphocholine; OLI-MB, oil layer inside MB.

RESULTS AND DISCUSSION

Contact angle measurement and surface energy calculation

Figure 2 shows a schematic of a droplet of oil at the air–water (modified with lipid) interface, and images of droplets at the air–water interface in the absence and presence of an adsorbed POPC lipid layer. The squalane contact angle decreased from 25° to 6° in the presence of POPC. The surface tension values of squalane reported in the literature vary between 25 and 30 mN m^{-1} (Refs. 46–50). While that of the lipid modified air–water interface is 26–27 mN m^{-1} for POPC at the collapse pressure[51–54]. The oil–water interfacial tension was calculated using the balance of the interfacial tensions for oil in contact with a water sub-phase and air spectator phase (see Equation (s1) from supplementary information). This was found to be 55 mN m^{-1} without lipid and $\leqslant$ 1.9 mN m^{-1} with POPC.

During OLI-MB formation, we form the MBs through flow focus 'pinch-off' of the gas in the presence of an aqueous solution containing LONDs with an average diameter of ~170 nm, as shown schematically in Figure 2c(i). If we assume a process in which LONDs adsorb then rupture to form a uniform oil layer at the water/gas interface (vide infra), then we expect of the order of 350 LONDs per MB. With this assumption, we can estimate the total surface energies for the initial starting state (Figure 2c(i)) and the different possible end configurations; (Figures 2c(ii) and (iii)). In going from the initial configuration (Figure 2c(i)) to the desired lipid-coated oil-shell surrounding a MB (Figure 2c(ii)) there would be a 2.6-fold reduction in the total surface free energy. In contrast, the scenario in which the LONDs agglomerate into a larger oil droplet, and the MB remains uncoated (Figure 2c(iii)), would lead to a similar total surface free energy to the initial configuration. The conclusion drawn here is that, since the OLI-MB structure was calculated to have the lower total surface free energy, it is energetically preferential as a final structure, and so formation of the structure is plausible.

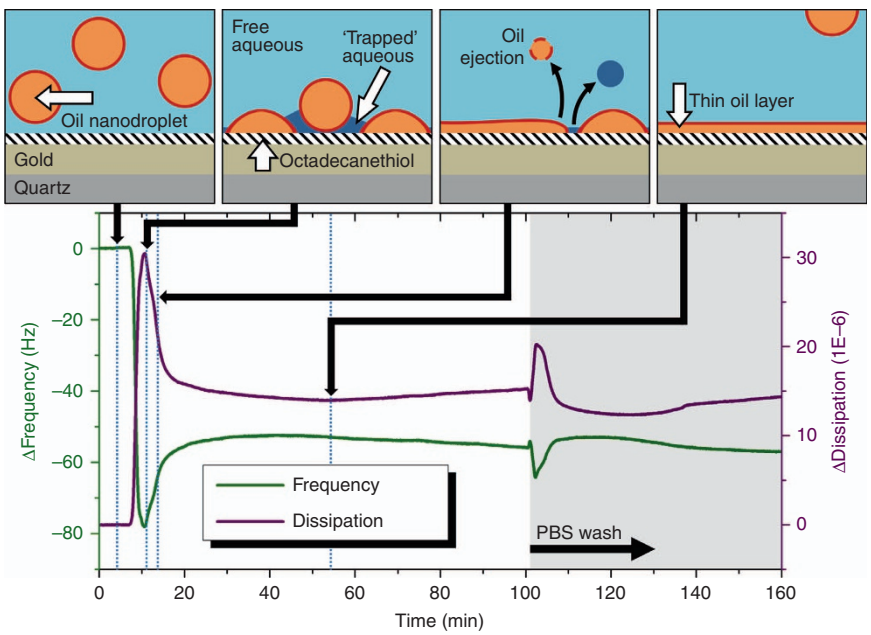

Figure 3 LOND interaction with an octadecanethiol SAM-coated gold surface. The changes in frequency and dissipation are shown for the seventh overtone of the QCM-D signal. The schematic shows the different stages in the LOND adsorption and spreading to form a uniform (thick) film. LOND, lipid oil nanodroplets; QCM-D, quartz crystal microbalance with dissipation.

doi:10.1038/micronano.2017.87

QCM-D: LOND spreading mechanics

To mimic the LOND/MB interaction, we performed QCM-D of LOND interactions with model hydrophobic surfaces. Figure 3 shows the changes in frequency (ΔF) and dissipation (ΔD) on interaction of LONDs with a hydrophobic QCM-D crystal. Initially, there was a rapid, negative increase in ΔF accompanied by a rapid, positive increase in ΔD, indicative of the absorption of LONDs and the formation of a heterogeneous, non-uniform surface layer, which couples strongly to the aqueous phase. Over the following ~10 min ΔF decreased and reached a plateau. Simultaneously, the ΔD decreased to a stable value of $\sim 15 \times 10^{-6}$. This behavior is similar to that of bilayer formation via vesicle adsorption and rupture on hydrophilic surfaces[55–57]. We propose a similar two-stage mechanism to explain our observations, (i) the attachment of LONDs (possibly partial wetting of the surface) followed by (ii) the slower spreading of droplets on the surface, leading to the detachment of entrapped water and possibly some oil. At the onset of washing the chambers, fresh LONDs were introduced to the surface, leading to a smaller increase in ΔF and ΔD, followed by the PBS wash, which resulted in the signal recovering to the 'before wash' level and further remaining stable. Changes in frequency provided an estimated value for the thickness of the oil layer formed during LOND rupture to be between 10 and 20 nm. This result gave an estimate of the order of 70 LONDs per MB. Recalculating the previous total surface free energies in respect to this still showed a 2.5-fold reduction when forming an OLI-MB from LONDs.

Microfluidic OLI-MB production

Figure 4a shows microfluidic OLI-MB production. Optimized production required low gas pressure (20–34.5 kPa), and aqueous flow rates between 20 and 25 μL min^{-1}, to prevent coalescence of the pinched off gas. This could be due to the slower adsorption and rupturing of LONDs at the gas–aqueous interface to stabilize

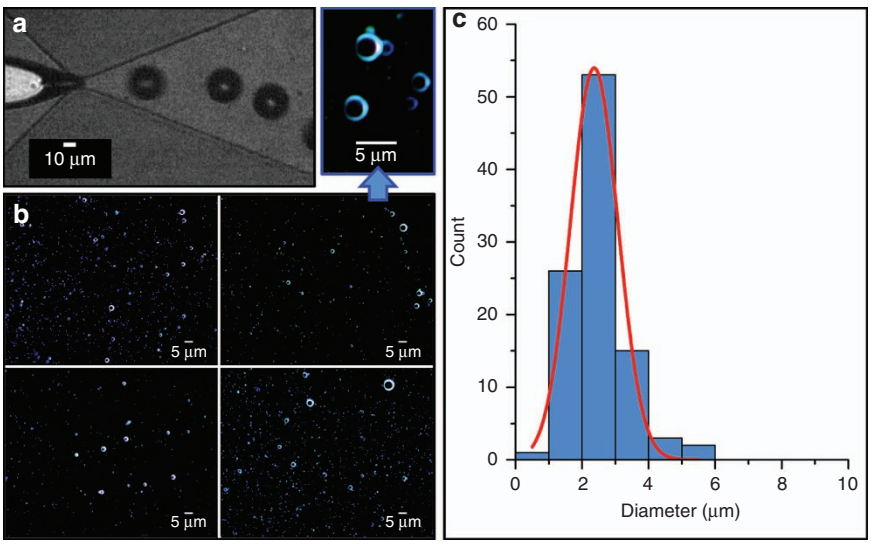

Figure 4 Images of OLI-MBs; (**a**) ×10 bright-field image taken during microfluidic production, 50 kfps, gas 34.5 kPa, LOND solution 24 μL min^{-1}, and (**b**) ×100 dark-field images taken after production, with zoomed and cropped inset (blue arrow), for (**c**) size and concentration analysis. LOND, lipid oil nanodroplets; OLI-MB, oil layer inside MB.

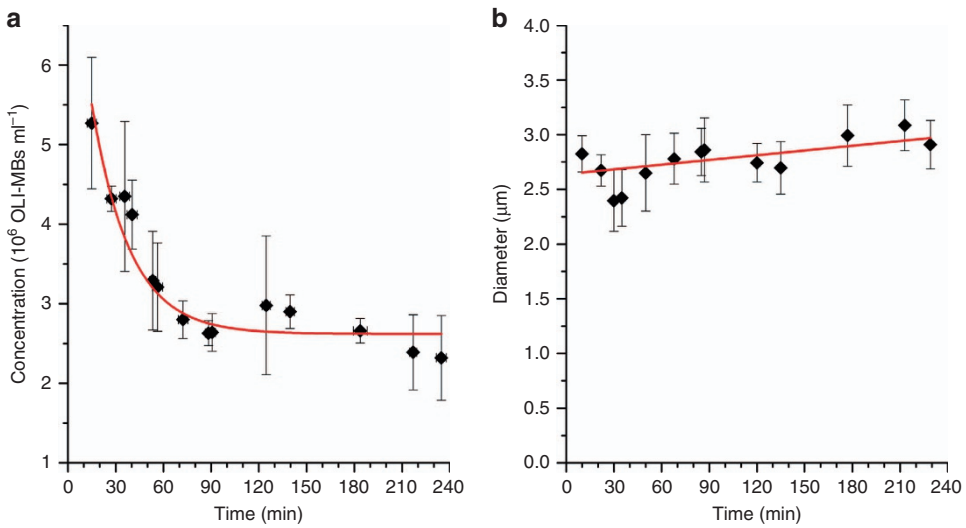

Figure 5 (**a**) Concentration and (**b**) diameter of squalane-POPC OLI-MBs as a function of time, at ~25 °C. The data presented represents the average over two OLI-MB production runs, and from three sample aliquots for each production. POPC, 1-palmitoyl-2-oleoyl-sn-glycero-3-phosphocholine; OLI-MB, oil layer inside MB.

the MBs, as depicted in Figure 1a. Production rates were ~5×10^3 OLI-MBs per s.

Figures 4b and c show off-chip imaging of the OLI-MBs and an associated size distribution. While OLI-MBs were routinely produced on-chip at 9.0 ± 1.8 μm diameter (s.d., 1.4 μm), off-chip imaging showed a repeatable reduction in MB size to ~0.3 times their initial size, giving OLI-MBs of 2.4 ± 0.3 μm (s.d., 1.6 μm) and a concentration of $6.2 \pm 0.8 \times 10^6$ MBs mL^{-1}. This size change was due to gas leakage from the interior of the MB after production. A MB's diameter effectively stabilizes when the lipid shell concentrates from an equilibrium state to being close packed at the collapse pressure. This effect has been shown previously on DPPC:DPPA:DPPE-PEG5000 MBs formed using FF devices, where MBs shrank to 0.39 times initial size[58].

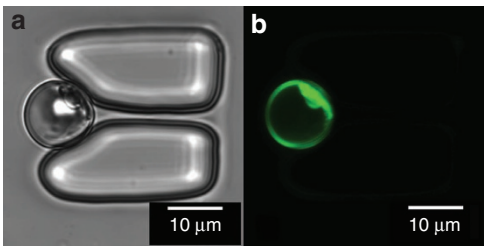

Figure 6 A microfluidic OLI-MB in a microfluidic cell-trap after washing with PBS. (**a**) Bright-field image and (**b**) fluorescence image of a MB incorporating DiI in the squalane shell. OLI-MB, oil layer inside MB.

Figure 5 shows the change in OLI-MB concentration and diameter over time. There was a sharp initial decrease in concentration over the first 90 min, after which the bubble concentration appeared stable for the duration of the measurement. During this period, the MB population showed a modest increase in size, presumably due to Ostwald ripening[29].

Figure 6 shows a trapped OLI-MB after the washing step to remove excess LONDs from the surrounding solution. The persistent fluorescent halo suggested that the oil component of the OLI-MBs was stable against shear forces and the removal of excess oil and lipid from the surrounding solution. All MBs observed in these traps after washing steps were recorded with some degree of fluorescent shell, indicating that the OLI-MB samples had been formed without any non-oil-MBs.

FRET LONDs: observing OLI-MB oil layer

Figure 7a shows a schematic for a FRET experiment to demonstrate the coalescence of LONDs and the mixing of their contents. Figure 7b shows the fluorescence signatures expected for three potential outcomes of LONDs at a MB's gas/water interface. Figure 7c shows the experimental acceptor emission following the interaction of LONDs containing donors and acceptors. FRET was shown to occur at the MB surface. As detailed by Figures 7a and b, observation of FRET signal provides evidence that the LONDs did adsorb and rupture at the MB interface, where oil and loaded fluorophores from both LOND populations mixed together. When compared to the QCM-D results for LONDs at a water–hydrophobic solid (as opposed to

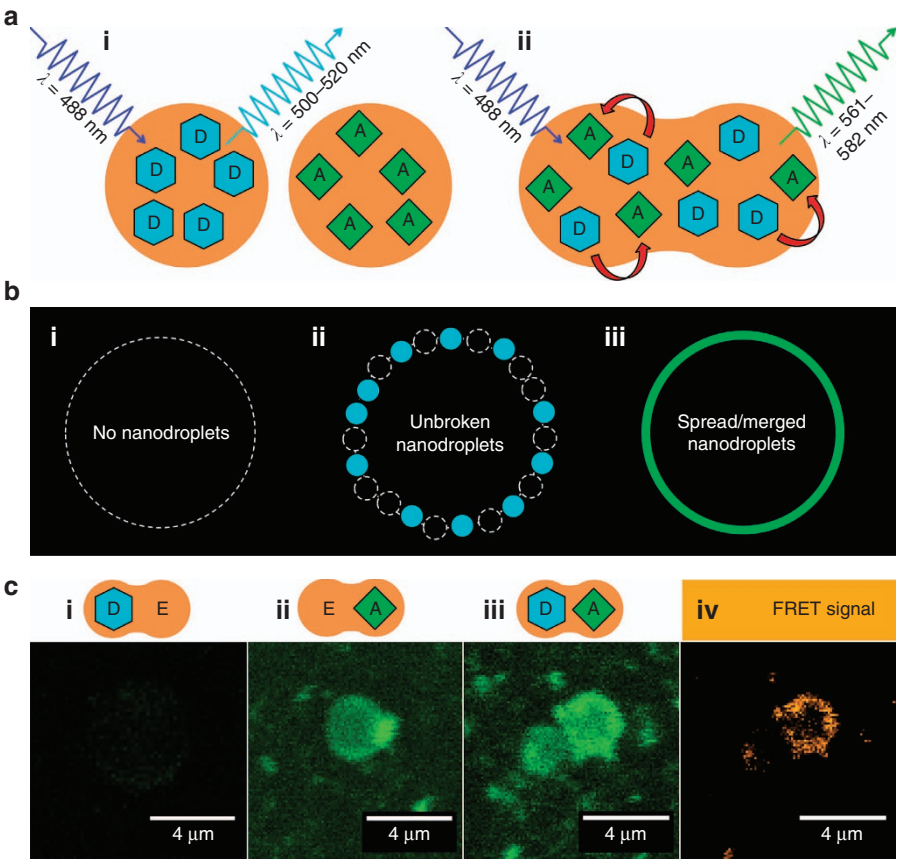

Figure 7 (**a** and **b**) Schematic of FRET-loaded LONDs for OLI-MB formation. Showing what would be observed if (**b**(i)) the LONDs contributed lipid for MB stabilization but no oil/fluorophore, donor (D) excitation leading to (**a**(i) and **b**(ii)) D emission if the nanodroplets remained stable at the MB surface, and (**a**(ii) and **b**(iii)) acceptor (A) emission if the nanodroplets merged/spread. (**c**) FRET OLI-MBs, formed from a combination of D, A, and non-fluorescent/empty (E) LONDs. All observation are of the A emission window, 561–582 nm. FRET signal image (**c**(iv)) calculated using Equation (1). FRET, fluorescence resonance energy transfer; LOND, lipid oil nanodroplets; OLI-MB, oil layer inside MB.

doi:10.1038/micronano.2017.87

gas) interface, these results appear to show a similar mechanism for the formation of a continuous oil layer around the gas core, resulting in OLI-MBs.

Additional work

Tripropionin OLI-MBs. Squalane is a non-polar oil with a very low water solubility[59]. Tripropionin is a partially water soluble triglyceride (3.07 mg mL^{-1} at 37 °C) used as flavoring agent[60]. By expanding the above work to form OLI-MBs from tripropionin LONDs, solubilization of a larger range of non-polar to partially polar drugs in to the oil phase would be possible. As such, the microfluidic OLI-MB production and wash steps have been repeated using tripropionin (Sigma-Aldrich, UK) LONDs. (See Supplementary Figure S1) Tripropionin OLI-MBs have been produced at 2.1 ± 0.1 μm diameter (s.d., 0.8 μm), though with a lower concentration of 10^4 OLI-MBs per milliliter.

CONCLUSION

We have presented a new approach to preparing MBs with an internalized oil component utilizing simple flow focussed microfluidics coupled with self-assembly. Squalane OLI-MBs were produced on-chip with diameters of 9.0 ± 1.8 μm that subsequently shrank and stabilized to a diameter of ~ 2.4 ± 0.3 μm (s.d., 1.6 μm), without any OLI-MBs shown above 8 μm. The final OLI-MB size has made this formation route of practical use for producing these MBs for clinical application. Off-chip OLI-MBs had a concentration of $6.2 \pm 0.8 \times 10^6$ OLI-MBs per mL. The mechanism of formation was via the adsorption and spreading of LONDs at the hydrophobic–hydrophilic interface during and shortly after MB 'pinch-off'. This process was mimicked using QCM-D, where the formation of a uniform oil layer was confirmed from changes in the frequency and dissipation. The continuous nature of the oil shell was confirmed using FRET imaging of MBs formed from two LOND species (one containing a donor species and the other an acceptor species). We have also shown that this is a general approach that can be used with different oil types. These architectures hold potential for the encapsulation and delivery of poorly water soluble and water-stable drugs. For potential clinical application of OLI-MBs, it may be advantageous to selectively separate the OLI-MBs from the excess LONDs they are formed in. This is possible based on the buoyancy of the different particles[61].

ACKNOWLEDGEMENTS

The authors thank the Leeds Microbubble Consortium for their continued support and discussions. Stuart Weston at University of Leeds, Physics workshop, for the construction of the manifolds for the microfluidic platform. We gratefully acknowledge the financial sponsorship of the EPSRC (Grant No. EP/K023845/1) and the EPSRC Centre for Doctoral Training in Molecular-Scale Engineering (Grant No. 1229421). SDE like to thank the NIHR-HTC for Colorectal Therapies, the MRC-CiC, and the Wellcome Trust ISSF Scheme for financial support. The data presented in this article are openly available from the University of Leeds Data Repository http://doi.org/10.5518/153.

COMPETING INTERESTS

The authors declare no conflict of interest.

REFERENCES

1 Straub JA, Chickering DE, Lovely JC *et al.* Intravenous hydrophobic drug delivery: A porous particle formulation of paclitaxel (AI-850). *Pharmaceutical Research* 2005; **22**: 347–355.
2 Kumar A, Sahoo SK, Padhee K *et al.* Reveiw on solubility enhancement techniques for hydrophobic drugs. *International Journal of Pharmaceutical Compounding* 2011; **2**: 1–7.
3 Tozer GM, Kanthou C, Baguley BC. Disrupting tumour blood vessels. *Nature Reviews Cancer* 2005; **5**: 423–435.
4 Rogstad DK, Herring JL, Theruvathu JA *et al.* Chemical decomposition of 5-aza-2'-deoxycytidine (Decitabine): Kinetic analyses and identification of products by NMR, HPLC, and mass spectrometry. *Chemical Research in Toxicology* 2009; **22**: 1194–1204.
5 Song B, Wu C, Chang J. Controllable delivery of hydrophilic and hydrophobic drugs from electrospun poly(lactic-co-glycolic acid)/mesoporous silica nanoparticles composite mats. *Journal of Biomedical Materials Research - Part B Applied Biomaterials* 2012; **100B**: 2178–2186.
6 Gupta S, Moulik SP, Lala S *et al.* Designing and testing of an effective oil-in-water microemulsion drug delivery system for *in vivo* application. *Drug Delivery* 2005; **12**: 267–273.
7 Aliabadi HM, Elhasi S, Mahmud A *et al.* Encapsulation of hydrophobic drugs in polymeric micelles through co-solvent evaporation: The effect of solvent composition on micellar properties and drug loading. *International Journal of Pharmaceutics* 2007; **329**: 158–165.
8 Ganta S, Devalapally H, Shahiwala A *et al.* A review of stimuli-responsive nanocarriers for drug and gene delivery. *Journal of Controlled Release* 2008; **126**: 187–204.
9 Muller RH, Mader K, Gohla S. Solid lipid nanoparticles (SLN) for controlled drug delivery—a review of the state of the art. *European Journal of Pharmaceutics and Biopharmaceutics* 2000; **50**: 161–177.
10 Hettiarachchi K, Lee AP, Zhang S *et al.* Controllable microfluidic synthesis of multiphase drug-carrying lipospheres for site-targeted therapy. *Biotechnology Progress* 2009; **25**: 938–945.
11 Stride E, Saffari N. Microbubble ultrasound contrast agents: A review. *Proceedings of the Institution of Mechanical Engineers, Part H: Journal of Engineering in Medicine* 2003; **217**: 429–447.
12 Chatterjee D, Sarkar K. A Newtonian rheological model for the interface of microbubble contrast agents. *Ultrasound in Medicine & Biology* 2003; **29**: 1749–1757.
13 Dalla Palma L, Bertolotte M. Introduction to ultrasound contrast agents: Physics overview. *European Radiology* 1999; **9**: S338–S342.
14 Peyman SA, Abou-Saleh RH, McLaughlan JR *et al.* Expanding 3D geometry for enhanced on-chip microbubble production and single step formation of liposome modified microbubbles. *Lab on a Chip* 2012; **12**: 4544.
15 Pitt WG, Husseini GA, Staples BJ. Ultrasonic drug delivery – a general review. *Expert Opinion on Drug Delivery* 2004; **1**: 37–56.
16 van Wamel A, Kooiman K, Harteveld M *et al.* Vibrating microbubbles poking individual cells: drug transfer into cells via sonoporation. *Journal of Controlled Release* 2006; **112**: 149–155.
17 Panje CM, Wang DS, Pysz MA *et al.* Ultrasound-mediated gene delivery with cationic versus neutral microbubbles: Effect of DNA and microbubble dose on *in vivo* transfection efficiency. *Theranostics* 2012; **2**: 1078–1091.
18 Liu Y, Miyoshi H, Nakamura M. Encapsulated ultrasound microbubbles: Therapeutic application in drug/gene delivery. *Journal of Controlled Release* 2006; **114**: 89–99.
19 Bekeredjian R, Chen S, Frenkel PA *et al.* Ultrasound-targeted microbubble destruction can repeatedly direct highly specific plasmid expression to the heart. *Circulation* 2003; **108**: 1022–1026.
20 Peyman SA, Abou-Saleh RH, Evans SD. Microbubbles for therapeutic delivery. *Therapeutic Delivery* 2013; **4**: 539–542.
21 McLaughlan J, Ingramy N, Abou-Saleh R *et al.* High-frequency subharmonic imaging of liposome-loaded microbubbles. IEEE International Ultrasonics Symposium, IUS; 21–25 July 2013; Prague, Czech Republic; 2013: 1501–1504; doi: 10.1109/ULTSYM.2013.0381.
22 Choi JJ, Pernot M, Brown TR *et al.* Spatio-temporal analysis of molecular delivery through the blood–brain barrier using focused ultrasound. *Physics in Medicine & Biology* 2007; **52**: 5509–5530.
23 Prausnitz MR, Mitragotri S, Langer R. Current status and future potential of transdermal drug delivery. *Nature Reviews Drug Discovery* 2004; **3**: 115–124.
24 Tinkov S, Coester C, Serba S *et al.* New doxorubicin-loaded phospholipid microbubbles for targeted tumor therapy: *In-vivo* characterization. *Journal of Controlled Release* 2010; **148**: 368–372.
25 Shih R, Bardin D, Martz TD *et al.* Flow-focusing regimes for accelerated production of monodisperse drug-loadable microbubbles toward clinical-scale applications. *Lab on a Chip* 2013; **13**: 4816.
26 Seo M, Gorelikov I, Williams R *et al.* Microfluidic assembly of monodisperse, nanoparticle-incorporated perfluorocarbon microbubbles for medical imaging and therapy. *Langmuir* 2010; **26**: 13855–13860.
27 Hettiarachchi K, Talu E, Longo ML *et al.* On-chip generation of microbubbles as a practical technology for manufacturing contrast agents for ultrasonic imaging. *Lab on a Chip* 2007; **7**: 463–468.
28 Talu E, Hettiarachchi K, Zhao S *et al.* Tailoring the size distribution of ultrasound contrast agents: Possible method for improving sensitivity in molecular imaging. *Molecular Imaging* 2007; **6**: 384–392.

29 Talu E, Hettiarachchi K, Powell RL *et al.* Maintaining monodispersity in a microbubble population formed by flow-focusing. *Langmuir* 2008; **24**: 1745–1749.
30 Peyman SA, McLaughlan JR, Abou-Saleh RH *et al.* On-chip preparation of nanoscale contrast agents towards high-resolution ultrasound imaging. *Lab on a Chip* 2016; **16**: 679–687.
31 Unger EC, McCreery TP, Sweitzer RH *et al.* Acoustically active lipospheres containing paclitaxel: a new therapeutic ultrasound contrast agent. *Investigative Radiology* 1998; **33**: 886–892.
32 Kooiman K, Böhmer MR, Emmer M *et al.* Oil-filled polymer microcapsules for ultrasound-mediated delivery of lipophilic drugs. *Journal of Controlled Release* 2009; **133**: 109–118.
33 Hettiarachchi K, Lee AP, Feingold SG *et al.* Ultrasonic analysis of precision-engineered acoustically active lipospheres produced by microfluidic. Proceedings - IEEE Ultrasonics Symposium; 20-23 Sept. 2009; Rome, Italy; 2009: 1302–1305; doi: 10.1109/ULTSYM.2009.5441565.
34 May DJ, Allen JS, Ferrara KW. Dynamics and fragmentation of thick-shelled microbubbles. *IEEE Transactions on Ultrasonics Ferroelectrics and Frequency Control* 2002; **49**: 1400–1410.
35 Lentacker I, De Smedt SC, Sanders NN. Drug loaded microbubble design for ultrasound triggered delivery. *Soft Matter* 2009; **5**: 2161.
36 Ahmad Z, Zhang H, Farook U *et al.* Generation of multilayered structures for biomedical applications using a novel tri-needle coaxial device and electrohydrodynamic flow. *Journal of the Royal Society Interface* 2008; **5**: 1255–1261.
37 Stride E, Edirisinghe M. Novel microbubble preparation technologies. *Soft Matter* 2008; **4**: 2350.
38 Zhang H, Meng H, Sun Q *et al.* Multi-layer microbubbles by microfluidics. *Scientific Research* 2013; **5**: 146–148.
39 Mico V, Charalambous A, Peyman SA *et al.* Evaluation of lipid-stabilised tripropionin nanodroplets as a delivery route for combretastatin A4. *International Journal of Pharmaceutics* 2017; **526**: 547–555.
40 Abou-Saleh RH, Peyman SA, Johnson BRG *et al.* The influence of intercalating perfluorohexane into lipid shells on nano and microbubble stability. *Soft Matter* 2016; **12**: 7223–7230.
41 Di Carlo D, Aghdam N, Lee LP. Single-cell enzyme concentrations, kinetics, and inhibition analysis using high-density hydrodynamic cell isolation arrays. *Analytical Chemistry* 2006; **78**: 4925–4930.
42 Aguilar-Castillo BA, Santos JL, Luo H *et al.* Nanoparticle stability in biologically relevant media: influence of polymer architecture. *Soft Matter* 2015; **11**: 7296–7307.
43 Chen H, Kim S, Li L *et al.* Release of hydrophobic molecules from polymer micelles into cell membranes revealed by Forster resonance energy transfer imaging. *Proceedings of the National Academy of Sciences of the USA* 2008; **105**: 6596–6601.
44 Xia Z, Liu Y. Reliable and global measurement of fluorescence resonance energy transfer using fluorescence microscopes. *Biophysical Journal* 2001; **81**: 2395–2402.
45 Zou P, Chen H, Paholak HJ *et al.* Noninvasive fluorescence resonance energy transfer imaging of *in vivo* premature drug release from polymeric nanoparticles. *Molecular Pharmaceutics* 2013; **10**: 4185–4194.
46 Kohler SPK, Reed SK, Westacott RE *et al.* Molecular dynamics study to identify the reactive sites of a liquid squalane surface. *Journal of Physical Chemistry* B 2006; **110**: 11717–11724.
47 Saecker ME, Govoni ST, Kowalski DV *et al.* Molecular beam scattering from liquid surfaces. *Science* 1991; **252**: 1421–1424.
48 Fowkes FM, Riddle FL, Pastore WE *et al.* Interfacial interactions between self-associated polar liquids and squalane used to test equations for solid-liquid interfacial interactions. *Colloids and Surfaces* 1990; **43**: 367–387.
49 Bascom WD, Cottington RL, Singleterry CR. Dynamic surface phenomena in the spontaneous spreading of oils on solids. *Advances in Chemistry* 1964; **43**: 355–379.
50 Phillips LF. A geometrical explanation for the enhanced small-scale roughness of a liquid surface. *The Journal of Physical Chemistry* B 2004; **108**: 1986–1991.
51 Pownall HJ, Pao Q, Brockman HL *et al.* Inhibition of lecithin-cholesterol acyltransferase by diphytanoyl phosphatidylcholine. *Journal of Biological Chemistry* 1987; **262**: 9033–9036.
52 Smith EC, Crane JM, Laderas TG *et al.* Metastability of a supercompressed fluid monolayer. *Biophyscial Journal* 2003; **85**: 3048–3057.
53 Domenech O, Torrent-Burgues J, Merino S *et al.* Surface thermodynamics study of monolayers formed with heteroacid phospholipids of biological interest. *Colloids Surfaces B Biointerfaces* 2005; **41**: 233–238.
54 Domènech Ò, Sanz F, Montero MT *et al.* Thermodynamic and structural study of the main phospholipid components comprising the mitochondrial inner membrane. *Biochimica et Biophysica Acta(BBA)-Biomembranes* 2006; **1758**: 213–221.
55 Richter RP, Brisson AR. Following the formation of supported lipid bilayers on mica: a study combining AFM, QCM-D, and ellipsometry. *Biophysical Journal* 2005; **88**: 3422–3433.
56 Dixon MC. Quartz crystal microbalance with dissipation monitoring: enabling real-time characterization of biological materials and their interactions. *Journal of Biomolecular Techniques* 2008; **19**: 151–158.
57 Keller CA, Kasemo B. Surface specific kinetics of lipid vesicle adsorption measured with a quartz crystal microbalance. *Biophysical Journal* 1998; **75**: 1397–1402.
58 Segers T, De Rond L, De Jong N *et al.* Stability of monodisperse phospholipid-coated microbubbles formed by flow-focusing at high production rates. *Langmuir* 2016; **32**: 3937–3944.
59 Spanova M, Zweytick D, Lohner K *et al.* Influence of squalene on lipid particle/droplet and membrane organization in the yeast Saccharomyces cerevisiae. *Biochimica et Biophysica Acta(BBA)-Molecular and Cell Biology of Lipids* 2012; **1821**: 647–653.
60 Royal Society of Chemistry. ChemSpider 2015; Available at http://www.chemspider.com/.
61 Mico V Developing microbubble-nanodroplet composites for enhanced hydrophobic drug delivery. PhD Dissertation, University of Leeds, Leeds, UK, 2017.

Supplementary Information for this article can be found on the *Microsystems & Nanoengineering* website (http://www.nature.com/micronano).

 doi:10.1038/micronano.2017.87